DOI: 10.61782/fa.2025.0360

FORUM ACUSTICUM EURONOISE 2025

EVALUATING THE APPLICABILITY OF STATISTICAL REVERBERATION THEORY IN ROOMS WITH VARYING COMPACTNESS AND MATERIAL DISTRIBUTIONS

Wouter Wittebol[1*] **Huiqing Wang**[1] **M.C.J. Hornikx**[1]

[1]Department of the Built Environment, Eindhoven University of Technology, P.O. Box 513, 5600 MB Eindhoven, The Netherlands

ABSTRACT

Statistical reverberation theory is a foundational framework for describing sound in enclosures, yet it often fails in practical scenarios, especially in rooms with non-compact geometries or uneven material distributions. This study investigates its validity by examining the absorption and scattering coefficients that govern the build-up and decay of non-specular sound fields. Backwards integrated impulse responses, generated with an image source model and a SPPS model (I-SIMPA), are used to extract coefficients via exponential fittings. These reconstructed coefficients are then compared to the conventional mean area-weighted coefficients across scenarios with varying compactness and material distributions. Results indicate that the fit improves with increasing compactness and that in terms of the spatial distribution of material properties scenarios with opposing walls of differing material properties show the poorest agreement. The findings of this study highlight the need to assess room characteristics before applying statistical reverberation theory or use an acoustic prediction model that is (partly) reliant on it.

Keywords: *Statistical reverberation theory, absorption coefficient, scattering coefficient, compactness, material distribution*

**Corresponding author*: *w.wittebol@tue.nl.*

1 Introduction

Concerns about the classical statistical reverberation models like Sabine [1] and Eyring [2] arise from their reliance on a room-averaged decay rate derived from the mean free path, which often fails to capture the manifold of decay phenomena present in realistic room acoustical scenarios [3]. The prerequisites that are necessary for the foundational assumptions of statistical reverberation theory to hold, namely that rooms are compact and that absorption properties are uniformly distributed, are not always met, particularly in the case of disproportionate or weakly mixing rooms, in which sound energy disperses slowly or unevenly, violating the assumptions of uniform energy density underlying statistical models. Many extensions to the classical reverberation models have been proposed over time to make better prediction for real rooms, for example [4–6]. Although these models have relaxed some of the restrictive assumptions of classical reverberation theory, they remain insufficient for fully capturing the complexities found in many practical real-world scenarios.

This work evaluates the applicability of the classical one-dimensional decay descriptions in a three-dimensional context. By decomposing the sound field into specular and non-specular components, we reconstruct average absorption and average scattering coefficients utilizing image source and particle-tracing impulse responses. Our goal is to determine when classical approaches remain valid and to quantify deviations using goodness-of-fit metrics and by comparing mean area-weighted absorption and scattering coefficients with those derived from impulse responses.

2 Used prediction methods

2.1 Compactness

A measure of an enclosures compactness, is to compare it to the most compact enclosure with the same volume *i.e.* a spherical enclosure. This measure is called the 'sphericity' (Ψ) and is defined as follows;

$$\Psi = \frac{\pi^{1/3}\,(6V)^{2/3}}{A} \tag{1}$$

with V the geometry's volume and A its surface area. For example a spherical enclosure has a sphericity of 1 and the most compact cuboid enclosure is a cube which has a sphericity of 0.81.

2.2 The Image Source Method

In this study, we utilize a pressure-based IS model for the special case of cuboid enclosures, as was described by Allen and Berkley [7], to model the specular part of the sound-field.

2.3 SPPS method

In order to model a total impulse response consisting of scattered as well as specularly reflected sound components we use the open source room acoustical simulation software I-Simpa with the build-in SPPS method. The SPPS method [8] used in I-Simpa [9] is a particle tracing method.

2.4 Statistical reverberation theory

Note that the idealized decay of sound energy in a room, based on classical statistical acoustics, is given by:

$$W_{\text{tot}}(f_i, t) = \left(1 - \bar{\alpha}(f_i)\right)^{c/l_c \cdot t}, \tag{2}$$

with $\bar{\alpha}$ the room-averaged absorption coefficient and l_c the mean free path of the room ($4V/S$). This W_{tot} can be split into a specularly (W_{s}) and non-specularly reflected part (W_{ns}),

$$W_{\text{tot}} = W_{\text{s}} + W_{\text{ns}}, \tag{3}$$

where the specularly reflected part is described as,

$$W_{\text{s}}(f_i, t) = \left[\left(1 - \bar{\text{s}}(f_i)\right) \cdot \left(1 - \bar{\alpha}(f_i)\right)\right]^{c/l_c \cdot t}, \tag{4}$$

with $\bar{s}$ the room-averaged scattering coefficient. The non-specularly reflected part is described as,

$$W_{\text{ns}}(f_i, t) = \left[1 - \left(1 - \bar{\text{s}}(f_i)\right)^{c/l_c \cdot t}\right] \cdot \left(1 - \bar{\alpha}(f_i)\right)^{c/l_c \cdot t}. \tag{5}$$

W_{tot}, W_{s} and W_{ns} are shown in Fig. 1 for a room with $\bar{\alpha} = 0.18$, $\bar{s} = 0.2$ and $l_c = 2.97\text{m}$.

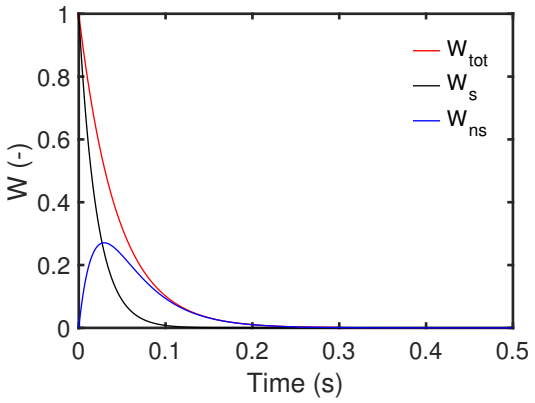

Figure 1. Temporal evolution of total (W_{tot}), specular (W_s), and non-specular (W_{ns}) reflected sound energy.

Note: All quantities are normalized with respect to the initial reflected energy, such that $W_{\text{tot}} = 1$ at $t = 0$, and are therefore dimensionless.

3 Method

In Sec.3.1, we describe the calculation of absorption and scattering coefficients within the framework of statistical reverberation theory. To assess how well these averaged coefficients represent a room's sound field, we compare them with absorption and scattering coefficients extracted from impulse responses generated using the sound particle simulation and the Image Source (IS) method. The procedure for obtaining these coefficients is detailed in Sec.3.2. We then discuss the analysis of these extracted coefficients in Sec. 3.3. Finally, this section concludes with an overview of the room acoustical scenarios that will be investigated.

3.1 Calculating mean area-weighted coefficients

In classical statistical reverberation theory, the calculation of sound decay curves relies on the volume, the total

boundary surface area of the enclosure, and the mean absorption coefficients for a given frequency. In this paper, we consider a frequency-independent case, where a single, representative mean area-weighted absorption coefficient $\bar{\alpha}$ is used, defined as:

$$\bar{\alpha} = \frac{1}{S_{\text{tot}}} \sum_{i=1}^{n} \alpha_i \cdot S_i, \tag{6}$$

where α_i is the random incidence absorption coefficient of each surface, and S_i is the area of each surface, with S_{tot} representing the total surface area. Similarly, the mean area-weighted scattering coefficient $\bar{s}$ can be computed as:

$$\bar{s} = \frac{1}{S_{\text{tot}}} \sum_{i=1}^{n} s_i \cdot S_i, \tag{7}$$

where s_i is the scattering coefficient for each surface.

3.2 Obtaining absorption and scattering coefficients utilizing impulse responses from sound particle simulation and image source method

In order to reconstruct absorption and scattering coefficients from impulse responses we adopt the following approach. We add a surface scattering coefficient to the image source model, which basically entails that upon each reflection in a surface besides the reduction due to sound absorption there is now an additional reduction according the scattering coefficient assigned to that surface. The result will be an impulse response that represents the **specular field** only (h_{s}).

We then simulate the same room only with a model that simulates the **total impulse response**, that is specular and diffuse part combined (h_{tot}). For that purpose we use the open source platform I-Simpa with its build in particle tracer engine (SPPS).

We now have two impulse responses, h_{tot} and h_{s}. Note that, within the framework of the statistical reverberation theory described in the previous section, $W_{\text{tot}} \approx h_{\text{tot}}^2$ and $W_{\text{s}} \approx h_{\text{s}}^2$. This similarity allows us to relate the energy decay of the total and specular components to the squared impulse responses. Furthermore, from h_{tot}^2 and h_{s}^2, we can also derive the non-specular portion of the sound field,

$$h_{\text{ns}}^2(t) = h_{\text{tot}}^2(t) - h_{\text{s}}^2(t). \tag{8}$$

3.2.1 *Utilizing Schroeder integration to smooth out reflection peaks*

The impulse responses from both the image source and SPPS simulations exhibit discrete reflection peaks. To smooth these peaks and derive a continuous energy decay curve (EDC), we apply Schroeder integration [10], which sums the reflections in reverse time. The resulting EDC is then normalized to its maximum value, as specified in ISO 3382-1 [11]. For the SPPS impulse response h_{tot}, we compute the energy decay as:

$$E_{h_{\text{tot}}^2}(t) = \frac{\int_t^\infty h_{\text{tot}}^2(\tau)\, d\tau}{\int_0^\infty h_{\text{tot}}^2(\tau)\, d\tau}, \tag{9}$$

and similarly for the squared ISM response with scattering h_{s}:

$$E_{h_{\text{s}}^2}(t) = \frac{\int_t^\infty h_{\text{s}}^2(\tau)\, d\tau}{\int_0^\infty h_{\text{s}}^2(\tau)\, d\tau}. \tag{10}$$

Performing the reverse-time integration on the theoretical description of W_{tot} and normalizing it to its definite integral from zero to infinity yields W_{tot} again. I.e. if,

$$W_{\text{tot}}(t) = (1-\bar{\alpha})^{tc/l_c}, \tag{11}$$

the reverse-time integral of W_{tot} is:

$$\int_t^\infty (1-\bar{\alpha})^{tc/l_c}\, d\tau = -\frac{1}{\ln(1-\bar{\alpha})} \cdot (1-\bar{\alpha})^{tc/l_c} \tag{12}$$

and the integral from 0 to infinity is:

$$\int_0^\infty (1-\bar{\alpha})^{tc/l_c} = -\frac{1}{\ln(1-\bar{\alpha})} \tag{13}$$

Thus, the energy decay for W_{tot} becomes:

$$E_{W_{\text{tot}}}(t) = \frac{-\frac{1}{\ln(1-\bar{\alpha})} \cdot (1-\bar{\alpha})^{tc/l_c}}{-\frac{1}{\ln(1-\bar{\alpha})}} = (1-\bar{\alpha})^{tc/l_c} = W_{\text{tot}} \tag{14}$$

Similarly, for the specular part of the energy decay, we get:

$$\int_t^\infty ((1-\bar{\alpha})(1-\bar{s}))^{tc/l_c} = -\frac{1}{\ln(1-\bar{\alpha}) + \ln(1-\bar{s})} \cdot ((1-\bar{\alpha})(1-\bar{s}))^{tc/l_c} \tag{15}$$

and the integral from 0 to infinity is:

$$\int_0^\infty ((1-\bar{\alpha})(1-\bar{s}))^{tc/l_c} = -\frac{1}{\ln(1-\bar{\alpha}) + \ln(1-\bar{s})} \tag{16}$$

$$E_{W_s} \frac{-\frac{1}{\ln(1-\bar{\alpha})+\ln(1-\bar{s})} \cdot ((1-\bar{\alpha})(1-\bar{s}))^{tc/l_c}}{-\frac{1}{\ln(1-\bar{\alpha})+\ln(1-\bar{s})}} = ((1-\bar{\alpha})(1-\bar{s}))^{tc/l_c} = W_s \quad (17)$$

The reverse-time integrated and normalized theoretical decay W_{tot} and W_{s} are self-similar—i.e., their normalized reverse time integrals retain the same functional form as the original expressions. This theoretical property proves useful when applied to impulse responses: by performing the same reverse-time integration and normalization on simulated responses such as h^2_{tot} or h^2_{s}, we obtain smooth energy decay curves (EDCs) suitable for exponential fitting. These fitted curves enable the estimation of absorption and scattering coefficients. Figure 2 shows the total energy decay $E_{h^2_{\text{tot}}}$, the specular part $E_{h^2_{\text{s}}}$, and the non-specular part $E_{h^2_{\text{ns}}}$, which resemble the theoretical decay curves in Fig. 1.

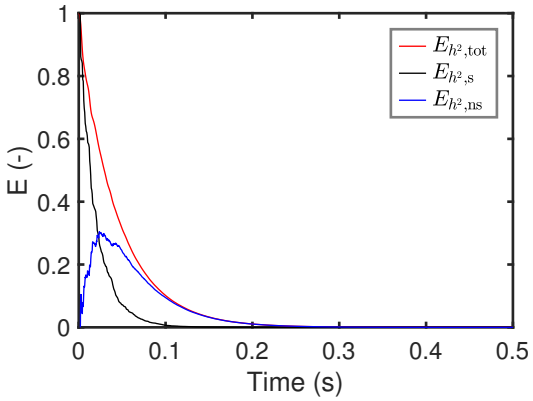

Figure 2. Total $E_{h^2_{\text{tot}}}$, specular $E_{h^2_{\text{s}}}$, and non-specular $E_{h^2_{\text{ns}}}$ parts of reflected energy ($\bar{\alpha} = 0.18, \bar{s} = 0.2, l_c = 2.97\text{m}$).

3.2.2 *Deriving the Specular-to-Total Energy Decay Ratio*

To extract a scattering coefficient, we require a decay curve that depends solely on scattering. While we already have an expression that depends on both absorption and scattering $E_{h^2_{\text{ns}}}$, it takes the form of a two-term exponential (Eq.5), which is, more difficult to fit robustly than a single-term exponential. Therefore, we seek an expression that isolates the effect of scattering. Within the framework of statistical reverberation theory, we can derive such a curve by taking the ratio of the specular part of the reflected energy to the total reflected energy. This results in:

$$W_\gamma(t) = \frac{W_{\text{s}}}{W_{\text{tot}}} = \frac{(1-\bar{s})^{\frac{c}{l_c}\cdot t}(1-\bar{\alpha})^{\frac{c}{l_c}\cdot t}}{(1-\bar{\alpha})^{\frac{c}{l_c}\cdot t}} = (1-\bar{s})^{\frac{c}{l_c}\cdot t} \quad (18)$$

Note that this ratio, $W_\gamma(t)$ represents a curve that depends solely on the scattering coefficient. Following this approach we now obtain a similar **ratio curve** by dividing the backwards-integrated ISM-IR curves $E_{h^2\text{s}}$ and $E_{h^2\text{tot}}$,

$$E_{h^2_\gamma}(t) = \frac{E_{h^2_{\text{s}}}(t)}{E_{h^2_{\text{tot}}}(t)} \quad (19)$$

This curve (E_γ) and the two backward integrated curves (E_{s} and E_{tot}) are shown in Fig. 3(a). As an example Fig. 3(b) shows the same curves only now obtained via Schroeder integration of the statistical curves W_{tot} and W_s. It is evident that in this case of a compact room with an homogeneous distribution of material properties on the boundaries these curves closely resemble the curves in Fig. 3(a). In contrast to the original IRs, which exhibited discrete peaks, we now have obtained curves that can be used for exponential fitting. We can utilize $E_{h^2_{\text{tot}}}$ to obtain a best fit absorption coefficient and we can utilize $E_{h^2_\gamma}$ to obtain a best fit scattering coefficient.

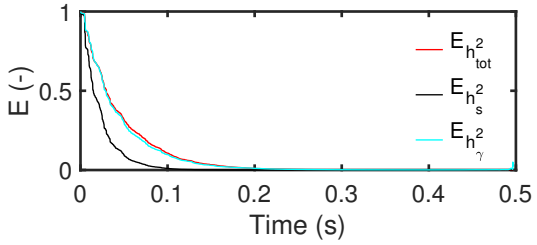

(a)

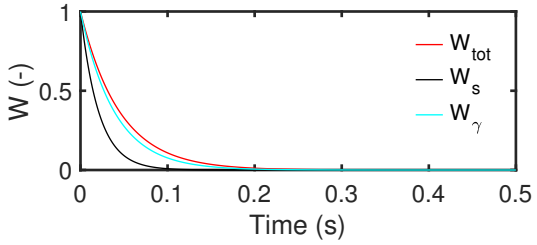

(b)

Figure 3. (a) Schroeder curves of IS-IR ($E_{h_s^2}$), SPPS-IR ($E_{h_{\text{tot}}^2}$) and their ratio $E_{h_\gamma^2}$ (b) W_{tot}, W_{s} and W_γ ($\bar{\alpha} = 0.18$ $\bar{s} = 0.2$, $l_c = 2.97$m).

3.2.3 *Exponential Fitting*

Absorption Coefficient We define $\bar{\alpha}_{\text{fit}}$ as the absorption coefficient estimated by fitting an exponential decay to $E_{h_{\text{tot}}^2}$ using MATLAB's curve fitting toolbox:

$$E_{\text{tot,fit}}(t) = A \exp\left(\ln(1-\bar{\alpha}_{\text{fit}})\frac{c}{l_c}t\right). \tag{20}$$

The scalar A is typically near 1; for ideal statistical curves, $A = 1$ yields an exact $\bar{\alpha}_{\text{fit}}$ with $R^2 = 1$. The fitting range is $[t_0, t_0 + t_{T_\beta}]$ with

$$t_0 = \frac{\|\vec{v}_s - \vec{v}_r\|}{c} \quad \text{and} \quad t_{T_\beta} = -\frac{4V}{cS}\frac{\ln(10^{\beta/10})}{\ln(1-\alpha)},$$

where t_0 is the arrival time of the direct sound and $\vec{v}_s$, $\vec{v}_r$ the position vector of the source and receiver respectively. β is the fitting range in dB, we used a 60 dB fitting range.

Scattering Coefficient Similarly, we define s_{fit} by fitting an exponential decay to $E_{h_\gamma^2}$:

$$E_{\gamma,fit}(t) = A \exp\left(\ln(1-\bar{s}_{\text{fit}})\frac{c}{l_c}t\right). \tag{21}$$

To account for rapid diffuse field build-up in case of high scattering, the fit is performed over $[t_0, t_0 + t_c]$ with

$$t_c = \frac{4V}{cS}\frac{\ln\left(1-\frac{P}{100}\right)}{\ln(1-\bar{s})},$$

where P is the percentage of non-specularity (set to $80\% \approx 1$dB).

3.3 Fit and Coefficient Analysis

3.3.1 *Goodness-of-fit Metrics*

We assess how well a single exponential decays can be fitted to $E_{h_{\text{tot}}^2}$ and $E_{h_\gamma^2}$ under varying compactness and boundary homogeneity by calculating the root mean square error (RMSE). This metric is displayed in box plots grouped by enclosure variant. We expect lower RMSE with increased room compactness and material homogeneity.

3.3.2 *Comparison of Statistical and Simulated Coefficients*

The differences between the reconstructed ($\bar{\alpha}_{\text{fit}}$, $\bar{s}_{\text{fit}}$) and the mean area-weighted coefficients ($\bar{\alpha}$,$\bar{s}$) are quantified by:

$$\bar{\epsilon}_\alpha = \frac{1}{n}\sum_{i=1}^{n}\left|\bar{\alpha}_{\text{fit},i} - \bar{\alpha}\right|, \quad \bar{\epsilon}_s = \frac{1}{n}\sum_{i=1}^{n}\left|\bar{s}_{\text{fit},i} - \bar{s}\right|.$$

Where n is the number of source receiver combinations. Their standard deviations indicate how closely the reconstructed coefficients match the averaged values. Impulse responses are obtained at various room positions to analyze the variability of the reconstructed coefficients around the room-average.

3.4 Room acoustical scenarios

3.4.1 *Characteristics of enclosures in terms of compactness*

In Table 1 the four cuboid enclosures chosen for this study are shown. These enclosures vary in terms of their compactness represented in terms of sphericity (Ψ) in the table.

Table 1. Characteristics of enclosures

Enclosure	Characteristics					
	Length (m)	Width (m)	Height (m)	Area (m^2)	Volume (m^3)	Ψ
No.1	12.65	2.71	2.60	148.31	89	0.65
No.2	9.83	3.48	2.60	137.61	89	0.70
No.3	7.66	3.87	3.00	128.53	89	0.75
No.4	4.46	4.46	4.46	119.60	89	0.81

3.4.2 *Characteristics in terms of distribution of material properties*

Several cases in terms of material property distribution are defined. These cases are outlined in Tab.2, the assigned wall numbers are shown in Fig.4. The absorption coefficients (α) are random incidence absorption coefficients.

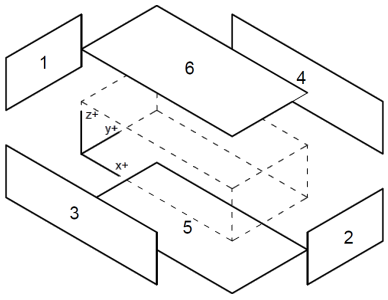

Figure 4. Assigned wall numbers for the cuboid enclosures used in the simulation model.

Table 2. Wall characteristics by variant

Variant		Wall number					
		1	2	3	4	5	6
I	α	0.18	0.18	0.18	0.18	0.18	0.18
	s	0.20	0.20	0.20	0.20	0.20	0.20
II	α	0.09	0.09	0.18	0.18	0.09	0.09
	s	0.10	0.10	0.20	0.20	0.15	0.15
III	α	0.09	0.18	0.09	0.18	0.09	0.18
	s	0.10	0.10	0.10	0.10	0.10	0.10
IV	α	0.18	0.18	0.32	0.32	0.25	0.25
	s	0.10	0.10	0.10	0.10	0.10	0.10

3.4.3 *Source and receiver positioning*

To investigate the influence of source and receiver positioning, IRs are simulated for a variety of source receiver combinations, these combinations are set forth in Tab.4.

Table 3. Mean area-weighted absorption and scattering coefficients per variant and enclosure.

Variant		Enclosure			
		1	2	3	4
I	$\bar{\alpha}$	0.180	0.180	0.180	0.180
	$\bar{s}$	0.200	0.200	0.200	0.200
II	$\bar{\alpha}$	0.130	0.123	0.122	0.120
	$\bar{s}$	0.167	0.162	0.159	0.150
III	$\bar{\alpha}$	0.135	0.135	0.135	0.135
	$\bar{s}$	0.100	0.100	0.100	0.100
IV	$\bar{\alpha}$	0.274	0.267	0.262	0.250
	$\bar{s}$	0.100	0.100	0.100	0.100

Table 4. Coordinates of source positions and receiver positions used in the different enclosures

Enc.	Crd.	Positions							
		R_1	R_2	R_3	R_4	R_5	R_6	S_1	S_2
1	x	3.41	6.08	9.74	2.91	6.58	9.74	4.99	11.32
	y	1.56	1.56	1.56	0.65	0.65	0.65	1.15	2.06
	z	1.20	1.20	1.20	1.20	1.20	1.20	1.50	1.50
2	x	2.71	4.67	7.62	2.21	5.16	7.62	3.94	8.85
	y	2.07	2.07	2.07	0.91	0.91	0.91	1.41	2.57
	z	1.20	1.20	1.20	1.20	1.20	1.20	1.50	1.50
3	x	2.17	3.58	5.99	1.66	4.08	5.99	3.12	6.95
	y	2.33	2.33	2.33	1.04	1.04	1.04	1.54	2.83
	z	1.20	1.20	1.20	1.20	1.20	1.20	1.50	1.50
4	x	1.37	1.98	3.59	0.86	2.48	3.59	4.09	1.92
	y	2.72	2.72	2.72	1.24	1.24	1.24	3.22	1.74
	z	1.20	1.20	1.20	1.20	1.20	1.20	1.50	1.50

4 Results and Discussion

4.1 Goodness-of-fit metrics for decay curve fitting

4.1.1 *Scattering*

Figure 5 shows the RMSE values for the $E_{\gamma,\text{fit}}$ variables over all source receiver combinations and variants. Looking at the RMSE values we can see that

the RMSE values are smallest for the case of the cubic room $\Psi = 0.81$, and that they increase when the compactness of the enclosure decreases with enclosure 4 resulting in the highest RMSE values. This confirms the expectations that the fit quality increases with increasing compactness of the room. Variant 4 shows the highest RMSE values among all the variants, for this variant sets of opposing walls have differing absorption properties.

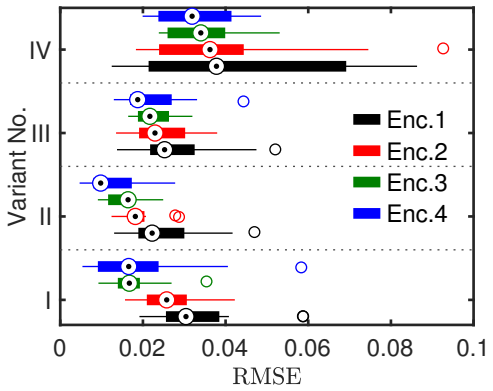

Figure 5. Boxplots of RMSE values of the $E_{\gamma,\text{fit}}$ over all source receiver combinations and variants 1-4.

4.1.2 *Absorption*

The RMSE values for absorption generally follow the expected trend of increasing with decreasing compactness. A notable exception is the second variant, this is probably because of the fact that the averaged scattering increases with decreasing compactness here, facilitating a more diffuse sound field. Variant 4 has the highest RMSE values , this is likely because in this variant sets of parallel walls have different decay rates due to having diverging absorptive characteristics assigned to them. Overall the RMSE values are relatively small compared to the ones obtained for scattering, indicating a overall good exponential fit. But a distinct dependence on the different variants and enclosure sizes is visible, and show similar behavior as the RMSE values obtained for the reconstructed scattering coefficients.

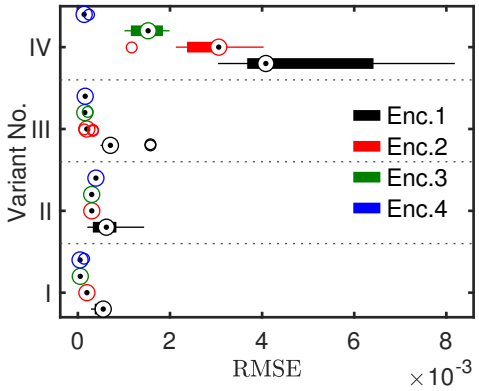

Figure 6. Boxplots of RMSE values of the $E_{\text{tot,fit}}$ over all source receiver combinations and variants 1-4

4.2 Comparison of mean area-weighted coefficients and reconstructed coefficients

4.2.1 *Scattering*

Figure 7 shows the average differences in the reconstructed scattering coefficients across all scenarios. It reveals that variant 2 exhibits the highest errors regarding scattering coefficients, caused by strong variations between wall sets. Variant 1 also shows larger deviations than variant 3, likely due to its higher average scattering coefficient, while variant 4's deviations are less pronounced than those in variant 2.

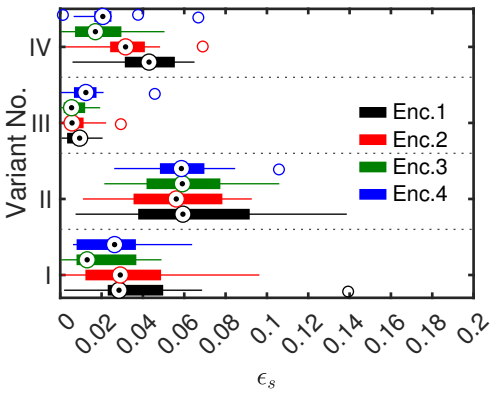

Figure 7. Boxplots of ϵ_s values over all source receiver combinations and variants 1-4

4.2.2 *Absorption*

Figure 8 shows that the largest errors between mean area-weighted and reconstructed absorption coefficients occur in variant 4, due to differing decay rates among the three wall sets. More compact enclosures show smaller deviations across all variants.

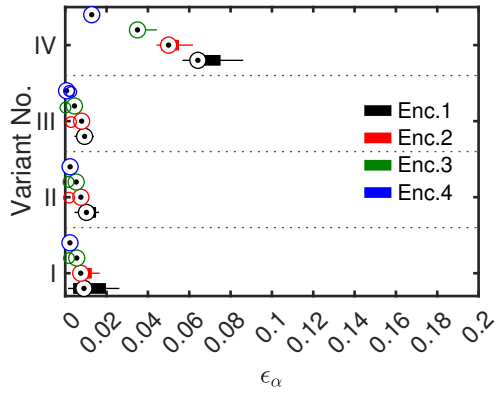

Figure 8. Boxplots of ϵ_α values over all source receiver combinations and variants 1-4

5 Conclusions

This study explored the limits of statistical reverberation theory by simulating impulse responses in rooms with varying compactness and material homogeneity using image source and SPPS models. Absorption and scattering coefficients were extracted via Schroeder integration and exponential fitting. Our findings indicate that compact enclosures conform more closely to the predictions of statistical reverberation theory, while discrepancies increase the less compact the space becomes or when the average absorption within the different sets of opposing walls are inconsistent.

6 References

[1] W. Sabine, *Collected papers on acoustics*. Dover Publications, first edition ed., 1964.

[2] C. F. Eyring, "Reverberation time in "dead" rooms," *Journal of the Acoustical Society of America*, vol. 1, no. 168, pp. 217–241, 1930.

[3] F. V. Hunt, "Remarks on the Mean Free Path Problem," *The Journal of the Acoustical Society of America*, vol. 36, pp. 556–564, Mar. 1964.

[4] D. Fitzroy, "Reverberation Formula Which Seems to Be More Accurate with Nonuniform Distribution of Absorption," *The Journal of the Acoustical Society of America*, vol. 31, pp. 893–897, July 1959.

[5] H. Kuttruff, "Reverberation and Effective Absorption in Rooms with Diffuse Wall Reflexions," vol. 35, 1976.

[6] H. Arau-Puchades, "An Improved Reverberation Formula," vol. 65, 1988.

[7] J. B. Allen and D. A. Berkley, "Image Method for efficiently simulating small-room acoustics," *The Journal of the Acoustical Society of America*, no. 65, p. 943, 1979.

[8] J. Picaut and N. Fortin, "SPPS, a particle-tracing numerical code for indoor and outdoor sound propagation prediction," 2012.

[9] J. Picaut and N. Fortin, "I-Simpa, a graphical user interface devoted to host 3D sound propagation numerical codes," 2012.

[10] M. R. Schroeder, "New Method of Measuring Reverberation Time," *The Journal of the Acoustical Society of America*, vol. 37, pp. 409–412, Mar. 1965.

[11] I. 3382-1:2009(en), "Acoustics — Measurement of room acoustic parameters — Part 1: Performance spaces," tech. rep., 2009.